Mechatronics 50 (2018) 177–188

Contents lists available at ScienceDirect

Mechatronics

journal homepage: www.elsevier.com/locate/mechatronics

A feedforward and feedback integrated lateral and longitudinal driver model for personalized advanced driver assistance systems

Scott Schnelle[a], Junmin Wang[a,*], Richard Jagacinski[b], Hai-jun Su[a]

[a] Department of Mechanical and Aerospace Engineering, Ohio State University, Columbus, OH 43210 USA
[b] Department of Psychology, Ohio State University, Columbus, OH 43210 USA

ARTICLE INFO

Keywords:
Driver modeling
Longitudinal and lateral motion
Advanced driver assistance systems

ABSTRACT

Advanced driver assistance systems (ADAS) are a subject of increasing interest as they are being implemented on production vehicles and also continue to be developed and researched. These systems need to work cooperatively with human drivers to increase vehicle driving safety and performance. Such cooperation requires the ADAS to work with the specific driver with some knowledge of the human driver's driving behavior. To aid such cooperation between human drivers and ADAS, driver models are necessary to replicate and predict human driving behaviors and distinguish among different drivers. This paper presents a combined lateral and longitudinal driver model developed based on human subject driving simulator experiments that is able to identify different driver behaviors through driver model parameter identification. The lateral driver model consists of a compensatory transfer function and an anticipatory component and is integrated with the design of the individual driver's desired path. The longitudinal driver model works with the lateral driver model by using the same desired path parameters to model the driver's velocity control based on the relative velocity and relative distance to the preceding vehicle. A feedforward component is added to the feedback longitudinal driver model by considering the driver's ability to regulate his/her velocity based on the curvature of his/her desired path. This interconnection between the longitudinal and lateral driver models allows for fewer driver model parameters and an increased modeling accuracy. It has been shown that the proposed driver model can replicate individual driver's steering wheel angle and velocity for a variety of highway maneuvers.

1. Introduction

Vehicle performance and safety are directly related to the control actions taken by the driver who acts as an adaptive, optimal decision-making controller for the vehicle. This human controller plays a significant role in terms of vehicle motion control, stability, driving safety, as well as energy consumption and emissions. Recent advances in vehicle active control and driver-assistance systems, e.g., electronic stability control (ESC), adaptive cruise control (ACC), lane departure warning (LDW), forward emergency braking (FEB), active lane change assist, and emergency steering assist [1] etc., have aimed to improve upon the control limitations of a human driver. The advanced driver assistance system (ADAS) success depends on the system's ability to work with each individual driver and share control with the driver in a way that complements the driver's driving style. Driver models offer a mathematical approach to define a driver's driving style/behavior and can interact with the ADAS.

Driver modeling is a broad research topic that spans many fields and disciplines. Automotive driver modeling can be split into two broad categories: longitudinal and lateral control modeling. This paper studies both driver's lateral and longitudinal motion controls and looks at their interconnection. For lateral driver steering behavior, research has been done in regards to modeling physical human characteristics such as sensory delays, limb movement, eye tracking, etc. [2–7]. Models for perception and behavioral aspects have been developed to supplement the basic physical driver models. Many of these steering models use compensatory transfer functions based on heading/lateral errors at a preview distance/time and some models include a feedforward, anticipatory term that is common in human drivers. There are other methods used to model driver steering behavior besides these physical models [8–20]. For a complete review of lateral driver models see [21]. The methods used to model the driver's lateral control of a vehicle are similar to the methods used to model the longitudinal control of a vehicle. Many models have been developed to describe not only traffic flow, which is not of a particular interest for the present research, but also car-following and collision-avoidance (CA) maneuvers, which are relevant for the present research. Physical based longitudinal driver models are one method researchers have employed to describe the

* Corresponding author.
E-mail address: wang.1381@osu.edu (J. Wang).

https://doi.org/10.1016/j.mechatronics.2018.02.007
Received 20 December 2016; Received in revised form 6 September 2017; Accepted 8 February 2018

speed control of a driver [22–30]. These models use physics based models with meaningful driver parameters such as acceleration limits, time delays, and following speeds/distances. Other methods including AutoRegressive with Exogeneous (ARX) models under the hybrid dynamical system (HDS) structure [32–36], rule-based decision field theory (RDFT) [37], action point theory [38–41] etc., are used to describe human driver longitudinal control of a vehicle. More recent driver models for ADAS applications include an improvement to the Intelligent Driver Model (IDM) called the Foresighted Driver Model [42] that balances driver risk and trip time, models that learn driver behavior and adjust to fit an individual vehicle/driver response [43,44] along with an Autogressive Input-Ouput HMM used to anticipate driving maneuvers a few seconds before they happen [45]. For a complete review of car-following methods, see [31].

Most of the aforementioned driver models have been designed and evaluated for standard, non-emergency lane-changing (LC) maneuvers. These maneuvers are beneficial to obtain a set of baseline parameters for the driver model; however, the major benefit of ADAS is to provide support during high-speed, dynamic, and challenging maneuvers where the driver is unable to provide the necessary control inputs to maintain a safe vehicle trajectory. In order for ADAS to seamlessly integrate control intervention with the driver during these emergency maneuvers, an accurate model of the driver is needed. Some research has been done in modelling driver steering behavior during CA maneuvers [46–52] and on modelling driver's vehicle speed control [53–55] to assist with automatic braking system for forward collision avoidance. However, in collision-imminent scenarios it has been shown that the distance required to make a lane change is shorter than that required to stop. Prynne and Martin [56] observed that in many cases only moderate steering input would be required to avoid the collision versus heavy braking and that drivers who steer to avoid collisions have a lower incidence of hitting an obstacle than drivers who brake. Drivers who brake and steer had the highest success rate of avoiding collisions. Lechner and Malaterre [57] stated that 45% of accidents in a case study could have been avoided with proper driver intervention. For 50% of these cases the correct intervention was steering input. This had led to the desire to develop active steering collision avoidance systems that incorporate steering intervention that could be autonomously steering the vehicle or by supplementing driver steering inputs. Choi and Yu [58] use a steering assist system that aids the driver by applying additional steer torque. This method is more readily accepted by drivers since there is less indication of system intervention than that in system where there is autonomous steering.

For these reasons the proposed driver model is able to model and predict not only the driver's steering wheel angle and velocity for standard, everyday maneuvers but also during emergency, collision-avoidance maneuvers. It does so using a longitudinal car-following model that takes into account the driver's safe following distance, desired relative velocity to the preceding vehicle, and their desired velocity along their individual path, along with a lateral driver model based on a compensatory transfer function along with a feedforward anticipatory subsystem. It also uses a method for determining each individual driver's desired target path in parallel with determining the driver model parameters, which is also missing in the previous driver model research. This variance in driver's desired path and trajectory generation has been observed in research [59–63]; however, none of these studies take into account each driver's desired path as part of the driver model. This feature allows the model to accurately depict how each individual driver steers and brakes/accelerates based on their perception of their own desired paths.

The rest of the paper is organized as follows. Section 2 introduces the structure of the combined driver model and desired path generation. In Section 3, the driving simulator and experimental procedure are introduced. Section 4 provides driving simulator human subject test results and driver steering and velocity control model to observed maneuvers. Section 5 concludes this paper.

2. Combined driver model

The combined lateral and longitudinal driver model proposed in this paper was selected because of its ability to accurately model the driver's steering wheel angle and vehicle velocity, with its relatively small set of meaningful parameters. The desired path parameters are shared amongst the lateral and longitudinal models. When the lateral model was used in previous research, it was necessary to assume a constant velocity or that the driver's speed was known in order to model the driver's anticipatory steering input [2,3]. With the addition of the longitudinal driver model, this assumption is no longer necessary.

2.1. Desired path

A baseline path for each type of maneuver can be constructed geometrically. The paths for the LC and CA maneuvers were generated using a second-degree polynomial fit. From this baseline centerline, each driver may interpret the maneuver differently based on their driving preference, i.e. driving in the center of the lane or left/right of center, entering into the maneuver sooner/later, changing lanes faster/slower, to generate his or her own desired centerline. The driver's desired path can be custom fit to their vehicle trajectory with 4 parameters for the LC/CA maneuvers as seen in Fig. 1.

The first parameter, Y_1, can be fit to the driver's first horizontal section of the maneuvers in the **Y** direction. The location of the start of

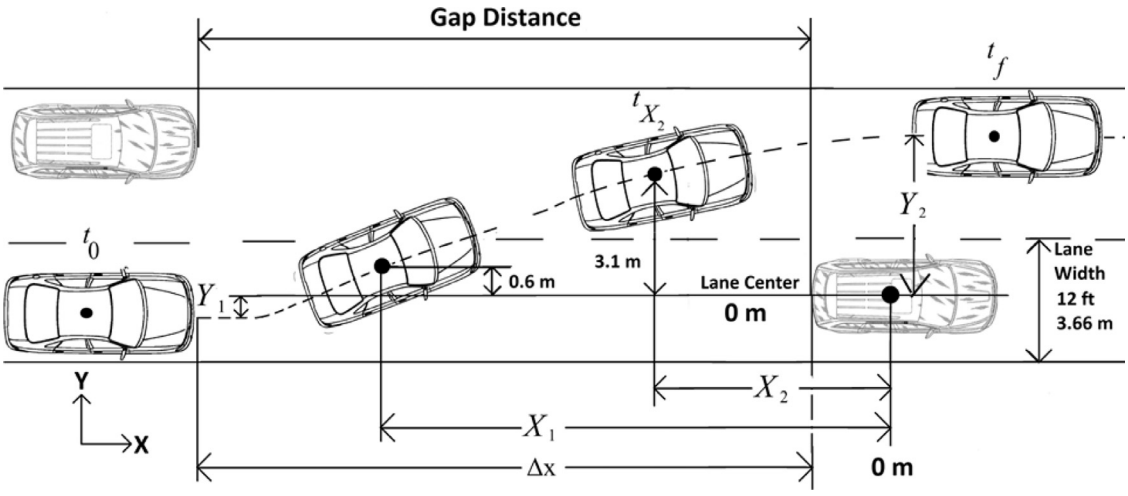

Fig. 1. Driver desired vehicle path.

the lane-change can be adjusted in the **X** direction by fitting parameter X_1. The end of the lane-change maneuver in the **X** direction can be adjusted with parameter X_2. The final horizontal section that represents the driver's target centerline in the adjacent lane can be adjusted in the **Y** direction with parameter Y_2. All of these parameters can be obtained from the driver's trajectory. The longitudinal desired path parameters, X_1 and X_2, are obtained for each driver by finding the following distance when the driver begins and ends the lane-change maneuver. The beginning of the lane-change maneuver was defined as when the vehicle center of gravity (CG) has a lateral position greater than 0.6 m from the lane centerline indicating that the vehicle is exiting the current lane. X_1 has been found to be similar to the location where the driver first applies the brake during LC/CA avoidance, if the brake is applied at all. In order to reduce the number of parameters, X_1 is used for the maneuver start location for the lateral and longitudinal models. As for the maneuver end, it is defined by when the driver's vehicle CG has a lateral position greater than 3.1 m from the previous lane, which is when the driver's entire vehicle fully enters the adjacent lane, completing the lane-change maneuver. The value of 3.1 m comes from subtracting the vehicle half-track width of 0.8 m from the lane width of 3.66 m along with adding a 0.24 m safety clearance allowance. The lateral parameters, Y_1 and Y_2, are obtained by taking the average **Y** position before the beginning, X_1, and after the end, X_2, of the lane-change maneuver, respectively. Once these desired path parameters are obtained, the desired path is generated using a second-degree polynomial fit.

The next component of the driver model is the combined driver model itself. The overall structure of the driver model is shown in Fig. 2.

2.2. Longitudinal driver model

The longitudinal driver model unifies a feedforward component and a feedback component.

2.2.1. Feedback longitudinal driver model

The feedback longitudinal driver model uses feedback in terms of relative following distance and velocity to model the driver's longitudinal speed control. The longitudinal model is based on the linear (Helly) models [29] and has the form:

$$a_{DM}(t) = C_1[\Delta x(t - T_d) - X_1] - C_2[\Delta v(t - T_d)], \quad (1)$$

where X_1 is the relative location where the driver begins the LC/CA maneuver from the driver's desired path, T_d is the driver's pure time delay in response to longitudinal stimuli, C_1 and C_2 are the driver's response gains to their desired following distance, $\Delta x(t\text{-}T_d) = X_1$, and velocity, $\Delta v(t\text{-}T_d) = 0$, respectively. C_1, C_2, and T_d are the three parameters to be calibrated. Using X_1 from actual data instead of it being an optimization parameter like it is in the original model [29] makes the model more predictable and consistent. The driver has a preferred following distance $\Delta x(t\text{-}T_d) = X_1$ and any Δx smaller than X_1 will result in the C_1 term of the driver model having a negative acceleration which corresponds to the driver braking to try to maintain his/her preferred following distance. The C_2 term is a look-ahead term to predict the driver's future Δx based on the current Δv. If the relative velocity is greater than 0, the Δv term will have a positive sign and since the C_2 sign is negative, this will result in the driver model having a negative acceleration which corresponds to the driver braking to maintain the preferred following distance since his/her vehicle is approaching the preceding one. The driver's feedback velocity profile, $v_{x,\,FB}$, was found by integrating the driver model acceleration starting at the maneuver's initial velocity.

Only using the feedback longitudinal driver model for the LC and CA maneuvers, Δx and Δv need to be defined after X_2, when the driver's vehicle is overtaking the preceding vehicle. To address this issue, the relative distance and velocity signals after the LC/CA maneuver were set to their initial, free-flow values defined as:

$$\Delta x(t_{X_2}\colon t_f) = \Delta x(t_0) \quad \Delta v(t_{X_2}\colon t_f) = \Delta v(t_0), \quad (2)$$

where t_0, t_{X2}, t_f are the time instants at the beginning of the recorded maneuver, at location X_2, and at the end of the recorded maneuver, respectively as seen in Fig. 1. The relative position and velocity signals were then smoothed with a moving-average filter to allow for a smooth transition between the car-following mode and the free-flow mode where the relative distance and velocity to preceding vehicle does not affect the driver's velocity. Eq. (2) only needs to be applied when solely

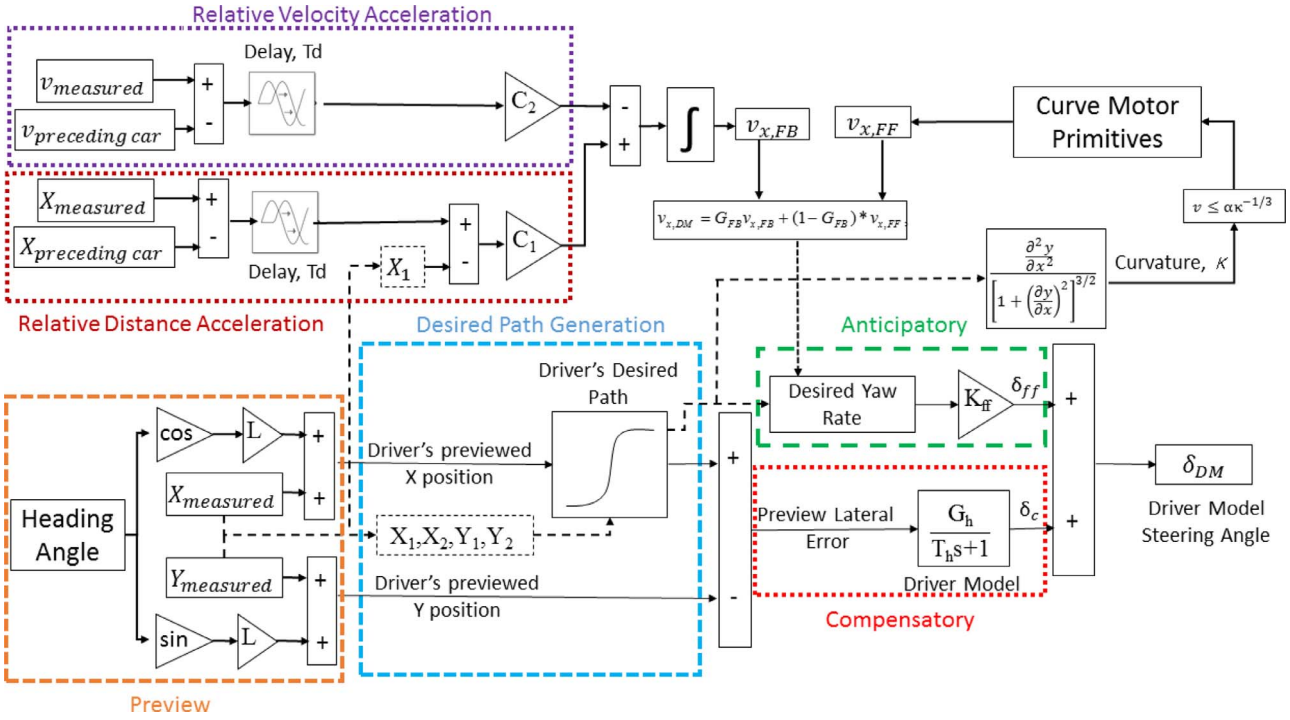

Fig. 2. Combined feedforward and feedback longitudinal and lateral driver model structure.

using the feedback longitudinal driver model and can be removed when combined with the feedforward longitudinal driver models as explained in the subsequent sections.

2.2.2. Feedforward longitudinal driver model

Many approaches to selecting driver speed in a curve restrict the lateral acceleration to a fraction of the tire cornering limit (μg) in order to find the limit speed in curves:

$$\frac{v^2}{r} = a_{lat} \leq k_s \mu g, \tag{3}$$

where v is the speed, r the path radius, μ the coefficient of friction, g is the acceleration due to gravity, and k_s is the driver's suitable safety margin. However, other studies [66–68] have shown that an inverse correlation between curvature and speed has been explained as a general feature of human movement. The methods proposed in those studies can be used to model this relationship, but the method that best fits to highway driving is the two-thirds power law [69]:

$$a_{lat} = \frac{\alpha^3}{v}, \tag{4}$$

with a model constant $\alpha = 3.34\ \mathrm{m}^{2/3}/\mathrm{s}$ to represent the median driver on urban and extra-urban roads. Each driver's individual α is found directly from their velocity profile at their desired path's maximum curvature. Substituting the equation for lateral acceleration around a curve of radius, r

$$a_{lat} = \frac{v^2}{r}, \tag{5}$$

into (4), one obtains the conditions that the speed must satisfy, given as a function of the trajectory curvature, $\kappa = 1/r$

$$v \leq \alpha \kappa^{-1/3}, \tag{6}$$

where the trajectory curvature is found from the individual driver's desired path by:

$$\kappa = \frac{\frac{\partial^2 y}{\partial x^2}}{\left[1 + \left(\frac{\partial y}{\partial x}\right)^2\right]^{3/2}}. \tag{7}$$

From this curvature-speed constraint, an optimal longitudinal control policy can be adapted for traveling close to a desired speed, v_d, as shown in Fig. 3. v_d is set equal to the driver's free-flow velocity at the beginning of the lane-change or collision-avoidance maneuver:

$$v_d = v(t_0) = v_0. \tag{8}$$

The task described in Fig. 3 can be expressed mathematically by considering a third-order dynamic system modeling the longitudinal kinematics:

$$\dot{s}(t) = v(t) \quad \dot{v}(t) = a(t) \quad \dot{a}(t) = j(t), \tag{9}$$

where j is the control input and s, v, and a are the states corresponding to longitudinal distance, velocity, and acceleration respectively. The goal is to find an input $j(t)$, which minimizes the following cost function J, with a free final time T:

$$J(j(\cdot), T) = \int_0^T w_T + j(t)^2 dt, \tag{10}$$

subject to the initial conditions and the final conditions:

$$s(0) = \Delta x_0 \quad v(0) = v_0 \quad a(0) = a_0, \tag{11}$$

$$s(T) = free \quad v(T) = v_d \quad a(T) = 0, \tag{12}$$

along with the velocity-curve constraints in (6) and the model equations in (9). The cost function, J, represents a trade-off between minimum time, the integral of $w_T = Tw_T$, and minimum input energy squared. This results in a competition between speed and accuracy inherent in any human movement. The maneuvers could be solved as a whole, from A–D in Fig. 3; however, the authors of [70] chose to break it down into simpler sub-problems that represent more basic motor tasks; one being negotiating a curve, A–B or A–C in Fig. 3, and another being achieving a desired speed, C–D or A–E in Fig. 3. These two types of motor tasks are called motor primitives.

2.2.2.1. Curve motor primitives. The first motor primitive is the curve motor primitive. It is used for negotiating a curved path. Eqs. (9)–(11) are still true, however the final condition in (12) is now:

$$s(T) = s_c \quad v(T) = v_c \quad a(T) = 0, \tag{13}$$

where v_c is the minimum speed at the curve apex, s_c, as shown in Fig. 4. The solution for the curve primitive is a 5th order polynomial to satisfy the initial and final conditions in (11) and (13):

$$s_c(t) = c_1 t + \frac{1}{2}c_2 t^2 + \frac{1}{6}c_3 t^3 + \frac{1}{24}c_4 t^4 + \frac{1}{120}c_5 t^5, \tag{14}$$

with:

$$\begin{aligned} c_1 &= v_0, \\ c_2 &= a_0, \\ c_3 &= -\frac{9a_0}{T} + \frac{60s_c}{T^3} - \frac{12(3v_0 + 2v_c)}{T^2}, \\ c_4 &= \frac{36a_0}{T^2} - \frac{360s_c}{T^4} + \frac{24(8v_0 + 7v_c)}{T^3}, \\ c_5 &= -\frac{60a_0}{T^3} + \frac{720s_c}{T^5} - \frac{360(v_0 + v_c)}{T^4}. \end{aligned} \tag{15}$$

The derivatives have the same structure:

$$\begin{aligned} v_c(t) &= c_1 + c_2 t + \frac{1}{2}c_3 t^2 + \frac{1}{6}c_4 t^3 + \frac{1}{24}c_5 t^4, \\ a_c(t) &= c_2 + c_3 t + \frac{1}{2}c_4 t^2 + \frac{1}{6}c_5 t^3, \end{aligned} \tag{16}$$

and the optimal control is quadratic:

$$j_c(t) = c_3 + c_4 t + \frac{1}{2}c_5 t^2. \tag{17}$$

The time T can be found by substituting (17) into (10) and

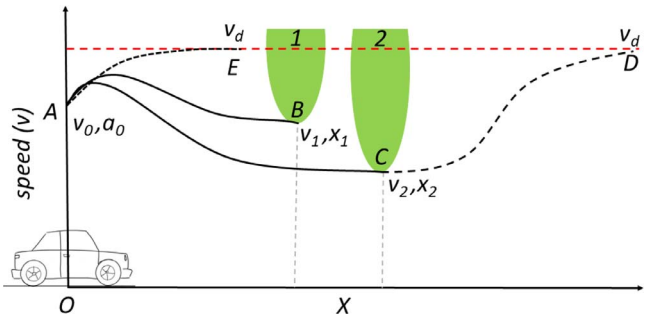

Fig. 3. Maneuver velocity planning based on road curvature and desired velocity.

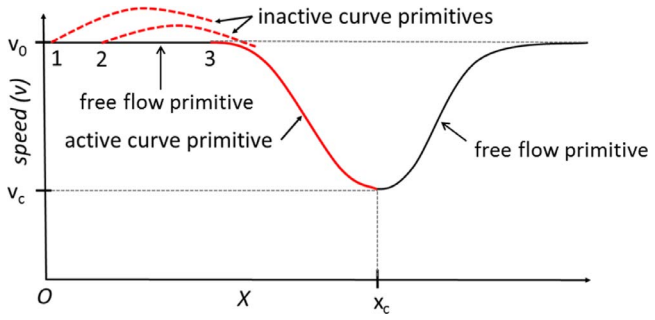

Fig. 4. Example of primitive selection based on (10).

minimizing, which yields:

$$J_c = Tw_T + \frac{9a_0^2}{T} + \frac{24a_0(3v_0 + 2v_c)}{T^2} + \frac{24(-5a_0s_c + 8v_0^2 + 14v_0v_c + 8v_c^2)}{T^3} - \frac{720s_c(v_0 + v_c)}{T^4} + \frac{720s_c^2}{T^5}. \quad (18)$$

It has to be noted that, for $T \to \infty$, J_c is asymptotic to T i.e., J_c–T. Conversely, for $T \to 0+$, J_c–T^{-5}. Therefore, there is at least one minimum for $T > 0$. By equating the derivative of J_c to zero, the following polynomial equation for the stationary points is obtained:

$$w_T T^6 - 9a_0^2T^4 - 48a_0(3v_0 + 2v_c)T^3 - 72(-5a_0s_c + 8v_0^2 + 14v_0v_c + 8v_c^2)\,T^2 + 2880s_c(v_0 + v_c)T - 3600s_c^2 = 0 \quad (19)$$

Inspection of the coefficients, based on Descartes' rule of signs, indicates that there may be either 1, 3 or 5 positive roots. Each local minimum represents, conceptually, a different strategy to meet the final conditions. Root 1 is the fastest strategy because it is associated to the smallest T, whereas root 3 is another option which would dilute the control over a longer time. The first root is selected to produce a motor primitive with a consistent meaning, often the global minimum. Thus, in all cases the first positive root of the polynomial (19) is considered and one can avoid comparing the cost function for all the roots. For computing the polynomial roots Matlab's *roots* function was used.

2.2.2.2. Free-Flow motor primitives. For this primitive, the final condition in (12) takes the form:

$$s(T) = free \quad v(T) = v_d = v_0 \quad a(T) = 0, \quad (20)$$

meaning that the target speed v_d is reached at a point that is determined by the driver's desired acceleration. The solution of the optimal control problem is similar to (14), (16), and (17), but with different coefficients, which are:

$$c_1 = v_0,$$
$$c_2 = a_0,$$
$$c_3 = \frac{6(v_d - v_0)}{T^2} - \frac{4a_0}{T},$$
$$c_4 = \frac{6a_0}{T^2} + \frac{12(v_0 - v_d)}{T^3},$$
$$c_5 = 0. \quad (21)$$

Note that, since $c_5 = 0$, the degrees of polynomials are reduced by one with respect to the previous case. Following the same logic as in the previous section, the optimal primitive duration T is found by minimizing (10) with substitution of the new expression for the free-flow jerk profile $j_f(t)$. A new polynomial equation is thus obtained:

$$w_T T^4 - 4a_0^2T^2 + 24a_0T(v_d - v_0) - 36(v_0 - v_d)^2 = 0. \quad (22)$$

This may have 1 or 3 real positive roots, except if $v_d = v_0$ and $a_0 = 0$, in which case the solution is uniform speed ($c_3 = 0$ and $c_4 = 0$). This is the case for all non-collision-avoidance, standard lane-changing maneuvers. The curvature of each driver's desired path is so large that the minimum curve speed, v_c, is larger than their desired speed, v_d. This means that the curvature is not a limiting factor in the driver's speed choice during a standard lane-change maneuver and the anticipatory longitudinal model results in a constant speed. When there are 3 roots, the global minimum is always taken.

2.2.2.3. Curve behavior. These two motor primitives above can be combined into a higher-level behavior. The central idea is that the motor primitives are constantly compared to select the input primitive that minimizes (10). For instance, when the vehicle is at point O in Fig. 3, three motor primitives are simultaneously generated: one for the free-flow goal and one for each of the two curves ahead. Then, the most appropriate primitive is selected a posteriori. Selecting one action means choosing one of the control outputs generated by the primitives, i.e., the $j_c(t)$ of the proper curve, or the flee-flow $j_f(t)$. Each action is represented by the three coefficients of $j(t)$. Action selection may thus be carried out primarily by comparing values of $j(t)$. For the lane-change and collision-avoidance maneuvers tested, the selection process consists of simply choosing the maneuver corresponding to the smallest $j(t)$, i.e., A–C in Fig. 3. With the above explanations, the curve behavior may thus be defined with the following pseudo-code:

Require: a_0, v_0, v_d, $\kappa(s)$, w_T
$j_f(s) \leftarrow$ FREEFLOW_PRIMITIVE(a_0, v_0, v_d, w_T)
$s_c \leftarrow$ FIND_MAXIMA($|\kappa(s)|$) ▶ s_c is a list
$n \leftarrow$ LENGTH(s_c)
for all s_c **do**
$v_{c,i} \leftarrow$ CURVE_SPEED($\kappa(s_{c,i})$)
$j_{c,i}(s) \leftarrow$ CURVE_PRIMITIVE(a_0, v_0, $v_{c,i}$, $s_{c,i}$, w_T)
end for
$j* \leftarrow \min\{j_f(t), j_{c,1}(t),\ldots,j_{c,n}(t)\}$
Select action with $j(t) = j* \rightarrow c_1^*, c_2^*,\ldots, c_5^*$
return $c_1^*, c_2^*,\ldots, c_5^*$

where a_0 and v_0 represent the initial state, $\kappa(s)$ the road curvature ahead, v_d and w_T the driver's goals, and c_i^* the coefficients of the active motor primitive. Finally, CURVE_SPEED calculates the minimum curve speed from the local curvature $\kappa(s_{c,i})$ from the Two-Thirds law, and CURVE_PRIMITIVE and FREEFLOW_PRIMITIVE are the result of case 1) and case 2) in the previous section, respectively. As an example, the curve behavior for the case of a vehicle approaching a curve with initial speed equal to the desired speed ($v_d = v_0$) is considered and illustrated in Fig. 4. Far from the curve, e.g., at points 1 and 2, the curve primitive would produce an initial acceleration because of the term w_T, as shown by the dotted curves. The selected action, is therefore free-flow ($v(t) = v_0 = v_d$), since $j_f(t) < j_c(t)$. However, as the vehicle comes closer to the curve, e.g., at point 3, the curve primitive no longer foresees initial acceleration. After point 3, the curve primitive is selected to decelerate until the curve apex (x_c, v_c). After this point, only the free-flow primitive exists, but now the speed is close to v_c, the desired speed is still v_d, and thus the free-flow primitive generates the post-curve speed-up. The point where the switching between primitives occurs (point 3) is influenced by w_T. The larger w_T, the later the switching.

2.2.3. Combined longitudinal driver model

The feedforward and feedback longitudinal driver models are combined to represent the real-world longitudinal control implemented by drivers. This consists of car-following behavior combined with anticipatory velocity tracking along the driver's desired path up to the lane-change and then desired velocity regulation after the maneuver completion. The two systems are combined using a position weighted transition gain, G_{FB}:

$$v_{x,DM} = G_{FB}v_{x,FB} + (1 - G_{FB})v_{x,FF}, \quad (23)$$

where G_{FB} is the weight the driver puts on the car-following behavior and (1-G_{FB}) is the weight the driver puts on the anticipatory velocity regulation along his/her desired path. The overall structure of the position weighted transition gain is shown in Fig. 5. This weighted transition fits into the existing structure of the driver model by using the individual driver's desired path parameters X_1 and X_2. Before the beginning of the lane-change or collision-avoidance maneuver, X_1, the driver uses a combination of car-following and regulates his/her desired velocity along the straight part of their desired path. As the driver executes the lane-changing or collision-avoidance maneuver, from X_1 to X_2, they rely less on car-following as the preceding vehicle becomes less

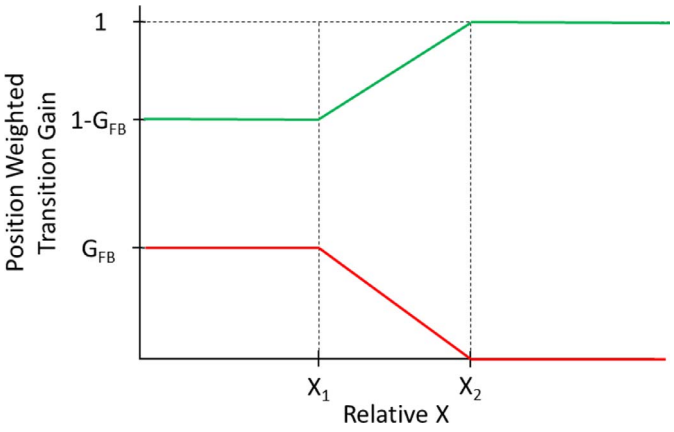

Fig. 5. Combined longitudinal driver model position weighted transition gain.

significant as they move into the adjacent lane and more on regulating their velocity along their desired path. After they have completed the lane-change or collision-avoidance maneuver, X_2, there no longer is a preceding vehicle for them to following since the vehicle they just passed is either behind them or in the adjacent lane, resulting in the driver only needing to regulate their speed based on their desired free-flow velocity. This formulation allows us to remove the definition of relative speed for the car-following model after the maneuver is completed from (2).

2.3. Lateral driver model

The steering model consists of a first-order compensatory transfer function with three parameters based on the model given by [20]:

$$\delta_c = (Y_d - Y_L)G_c(s) = (Y_d - Y_L)\frac{G_h}{1 + T_h s}, \tag{24}$$

where δ_c is the driver's compensatory steering wheel angle, $Y_d - Y_L$ is the error between the desired path and that of the vehicle at the driver's preview distance L ahead, G_h is the driver's steer proportional gain, and T_h is the driver's lag time constant. The preview distance is projected from the vehicle's current heading angle. This allows for the model to have a predictive ability that is common in human driver models as it reflects a human driver's ability to look ahead and plan a path accordingly. The compensatory subsystem of the driver model is supplemented with a feedforward subsystem with only one parameter that takes into account the driver's ability to anticipate the desired road geometry. The feedforward subsystem has transfer function:

$$\delta_{ff} = K_{ff}\dot{\psi}_d, \tag{25}$$

where δ_{ff} is the driver's feedforward steering angle,K_{ff} is the driver's feedforward gain and $\dot{\psi}_d$ is the desired yaw rate. The desired yaw angle,ψ_d, is calculated by:

$$\psi_d = a\tan\left(\frac{Y_d}{X_d}\right), \tag{26}$$

The desired yaw rate can then be found based on the desired yaw angle:

$$\dot{\psi}_d = \frac{\Delta\psi_d}{\Delta x / v_{DM}}, \tag{27}$$

where Δx is the distance travel between time steps, $\Delta\psi_d$ is the change in desired yaw angle between time steps, and $v_{x,\ DM}$ is the velocity from the longitudinal driver model. These two subsystems can be combined to result in the driver model's overall steering wheel angle, δ_{DM}:

$$\delta_{DM} = \delta_c + \delta_{ff}. \tag{28}$$

2.4. Optimization of model parameters for individual drivers

With the driver model in place and the four parameters of the desired path generation obtained from the vehicle trajectory, the three driver acceleration model parameters can be optimized to minimize the cost function: s

$$J = \int_0^T |v_{x,DM} - v_{x,r}|dt, \tag{29}$$

where v_r is the recorded driver velocity from the driving simulator test. The four driver steering model parameters can then also be optimized to minimize the cost function:

$$J = \int_0^T |\delta_{DM} - \delta_r|dt, \tag{30}$$

where, δ_r is the recorded driver steering wheel angle signal.

The Matlab Global Optimization Toolbox was used to find a global minimum for these nonsmooth objective functions. This optimization is done offline with an average processing time of 11 min per maneuver.

3. Experimental setup

To determine each driver's path and driver model parameters, driving simulator experiments are used to overcome the time, cost, and safety constraints of a real vehicle test. Another advantage of using a driving simulator is that it gives complete access to all vehicle states which are impossible to measure directly in a real vehicle test. A 10-DOF vehicle dynamic model allows access to manipulate and record all of the vehicle dynamics.

3.1. Driving simulator

A fixed-base driving simulator is used for the driving experiments. The simulator is a semi-immersive virtual environment based on the Christie digital Holostage mini CAVE system consisting of two rear projectors, two screens, five speakers, a driver seat, a steering wheel, and accelerator/brake pedals as seen in Fig. 6. The driver's inputs are measured through the steering wheel angle and accelerator/brake pedal positions. These inputs are fed into a 10-DOF ground vehicle mathematical model in Simulink where all of the vehicle states are recorded and saved for the estimation of the model parameters. Three outputs of this model (*X, Y*, and yaw angle) are then sent via a dedicated transmission control protocol socket channel to Vizard, a virtual reality (VR) software which renders visualization of the vehicle to the virtual environment. A human driver can then complete the control loop and sense the vehicle motions from the visual display and audio feedback and react accordingly.

3.2. Vehicle model

The vehicle model used and all of the vehicle equations of motion are based on the model in [64]. The vehicle model is described in detail and validated in [2] and will only be briefly introduced in this paper. The vehicle being modeled has vehicle properties of a D-class sedan and is modeled with a 10-DOF vehicle model. 6 DOF come from the vehicle *X, Y*, yaw, roll, pitch motions, and a suspension lateral load transfer equation. The other 4 DOF come from the tire dynamics which are calculated using the magic formula tire model [65].

3.3. Maneuvers

A summary of each driving scenario's parameters can be found in Table 1. Before the data were recorded, the drivers were each given an introductory course consisting of each of the tested maneuvers. Once the drivers were familiarized with the driving simulator and each maneuver, the test procedure began. The driving scenarios were in a

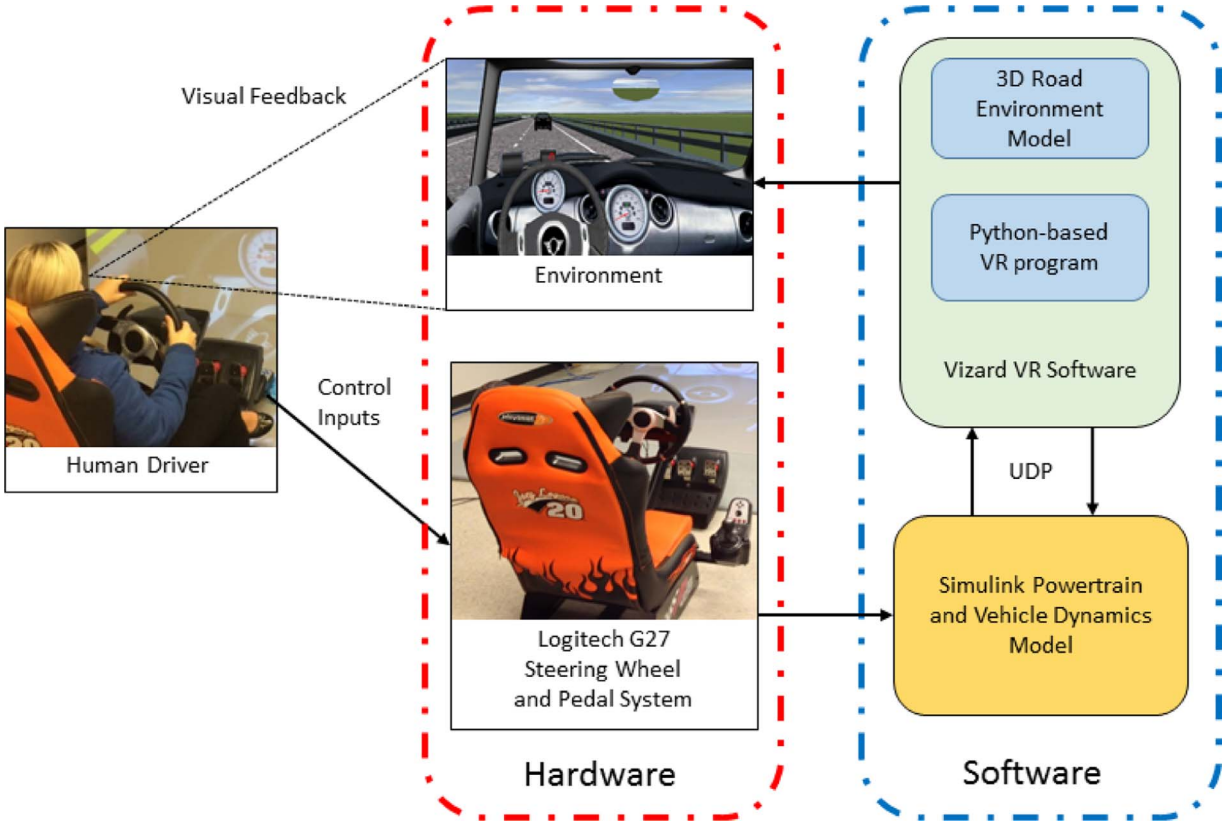

Fig. 6. Virtual reality driving simulator structure.

Table 1
Test maneuvers.

Scenario	Gap distances (m)	Traffic speeds (mph)
Highway lane change	55	50
	43	47.5
	37	45
	31	–
Highway collision avoidance	43	50
	37	47.5
	31	45

simulated highway course with traffic. The speed limit was posted at 55 mph, and the drivers were instructed to drive as they would on a normal highway. The combined scenario consisted of preprogrammed cars that were spaced at different distances between each other (gap distance) and that were moving at various speeds (see Table 1). Since all of the vehicles were driving at speeds below the posted 55 mph speed limit, the driver had to perform a lane-change maneuver and pass them. However, some of the vehicles were programmed to suddenly brake when the driver reached a certain following distance, and the driver needed to steer to avoid a collision with the preceding vehicle. The collision-avoidance maneuvers were set up in such a way that steering was necessary for collision avoidance because the preceding vehicle decelerated at a rate of -0.9 g and the driver would not be able to stop in time to avoid a collision for the given speed, following distance and road coefficient of friction. The adjacent lane was open to the driver to avoid the preceding braking vehicle. The driver's visual cue was the preceding car's brake lights. For each highway maneuver, following distance, and speed in Table 1, four sets of data were collected. This resulted in 21 different combinations of speed, following distance, and maneuvers each being repeated four times for a total of 84 recorded maneuvers.

4. Driver model results

4.1. Feedback longitudinal driver model results

Once the drivers completed all of the maneuvers the data were split and then the model fit was optimized. The driver steering wheel angle and vehicle velocity fits were evaluated. The sample size for this experiment was 20 subjects, and their demographic information, fitting error can be seen in Table 2. More driver data, including more diverse

Table 2
Feedback driver model average velocity error.

Driver	Gender	Age	Average velocity error (m/s)	
			LC	CA
1	M	26	0.48	0.50
2	F	25	0.62	0.56
3	M	27	1.02	0.75
4	M	25	0.72	0.42
5	M	24	0.54	0.65
6	M	27	0.39	0.60
7	M	28	1.15	0.72
8	M	27	1.08	0.56
9	M	26	0.44	0.14
10	M	25	0.24	0.16
11	M	41	0.53	0.53
12	F	40	0.33	0.52
13	M	31	0.66	0.45
14	F	31	0.33	0.38
15	F	28	0.27	0.12
16	M	33	0.34	0.16
17	F	28	0.40	0.42
18	M	27	0.43	0.45
19	M	26	0.47	0.48
20	M	26	0.25	0.88
AVG	**5F/15M**	**28.5**	**0.53**	**0.47**

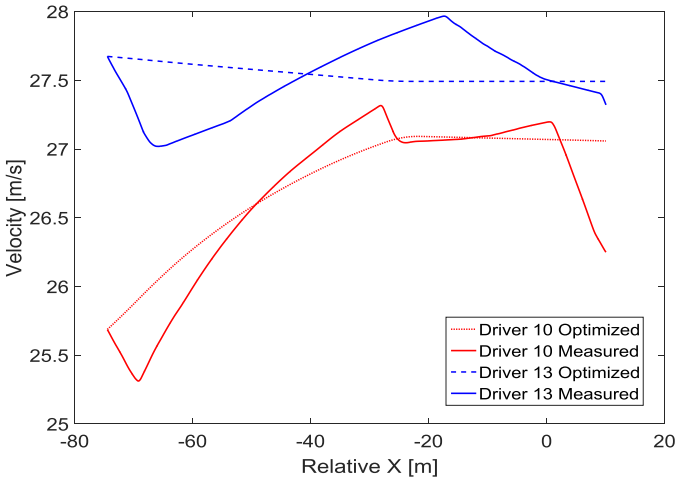

Fig. 7. Feedback longitudinal driver model LC velocity fits.

data in terms of driver's gender and age, may further enhance the model.

Matlab's *goodnessOfFit* function was used to evaluate the steering wheel angle fits. The cost function used to determine the goodness of fit was the normalized mean square error:

$$fit(i) = 1 - \left\| \frac{xref(:,i) - x(:,i)}{xref(:,i) - mean(xref(:,i))} \right\|^2. \tag{31}$$

To evaluate the velocity profile fits, the average error was used. The *goodnessOfFit* metric was not used because for some of the maneuvers, such as the LC maneuvers, the driver's maintained a constant speed with some small deviations that the model does not capture resulting in a bad fit when in reality the model was able to capture the overall velocity profile, as shown in Fig. 7.

The proposed driver model is able to approximate each driver's steering wheel angle and velocity for each combination of following distance, speed, and maneuver. A sample comparing drivers with different driving styles for the same maneuver can be seen in Figs. 7 and 8. There is a large difference in velocity and steering wheel angle when comparing driver to driver and maneuver to maneuver. Some driver model parameters optimized for different drivers are shown in Figs. 9–11. Such discrepancies between maneuver and driver-specific driver model parameters necessitate a personalized predictive driver model.

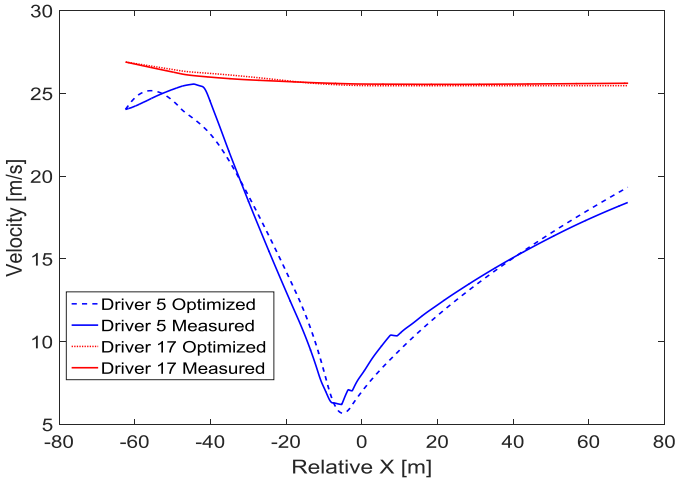

Fig. 8. Feedback longitudinal driver model CA velocity fits.

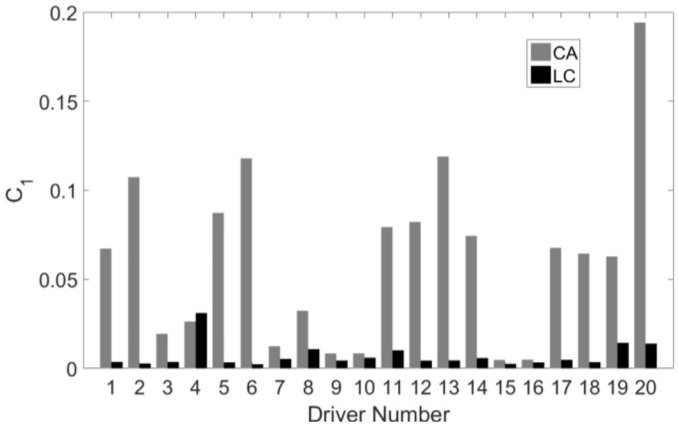

Fig. 9. Feedback longitudinal driver model parameter C_1.

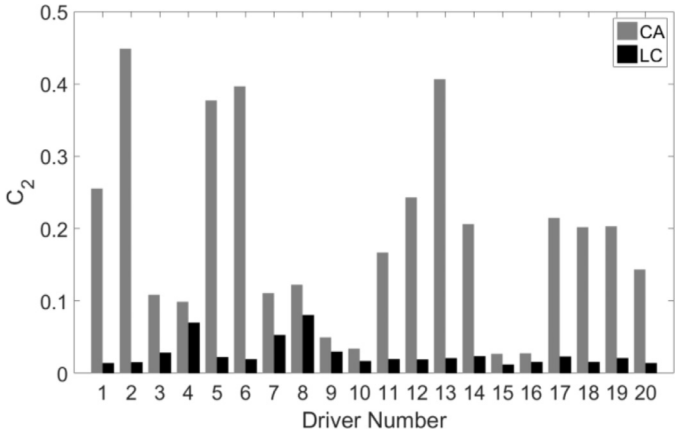

Fig. 10. Feedback longitudinal driver model parameter C_2.

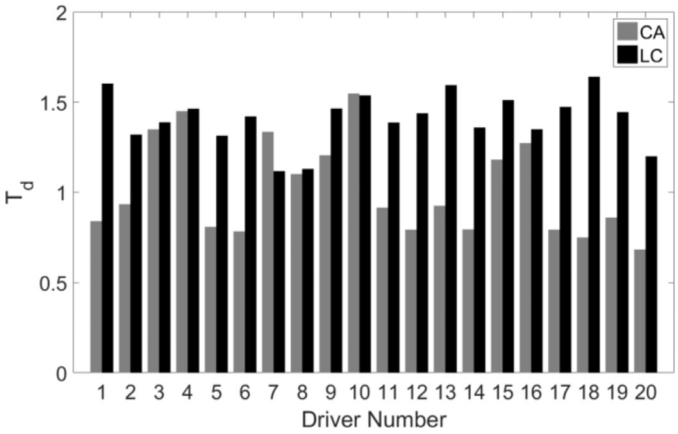

Fig. 11. Feedback longitudinal driver model parameter T_d.

4.2. Feedforward longitudinal driver model results

The feedforward longitudinal driver model velocity can be seen in Figs. 12 and 13. As previously mentioned, for the standard lane-change maneuvers the feedforward driver model would result in a constant velocity since $v_d = v_0$ and $a_0 = 0$. The curvature of each driver's desired path is so large that the minimum curve speed, v_c, is larger than their desired speed, v_d. This means that the curvature is not a limiting factor in the driver's speed choice during a standard lane-change maneuver and the curve motor primitive is never active.

However, for the collision avoidance maneuvers, the curve motor primitive is activated due to the increased curvature of the driver's

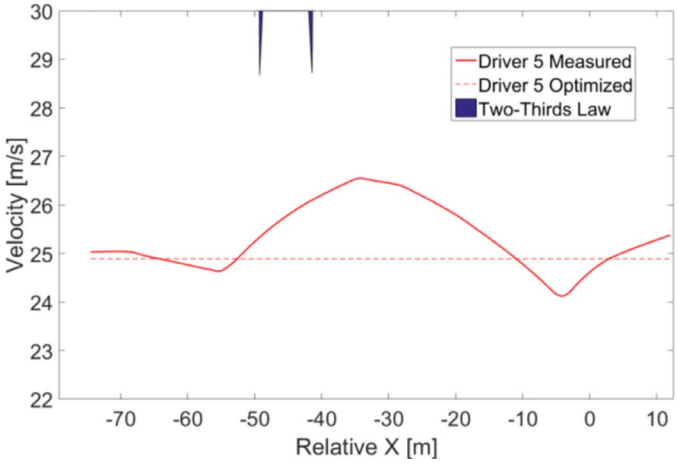

Fig. 12. Feedforward longitudinal model for a LC maneuver.

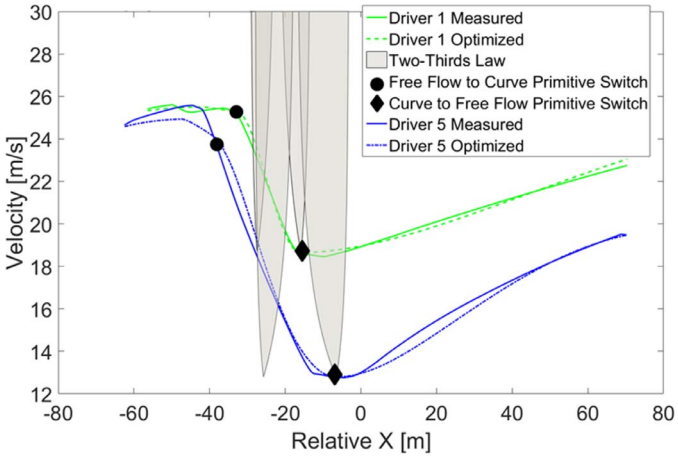

Fig. 13. Feedforward longitudinal model for a CA maneuver.

Table 3
Feedforward driver model average velocity error.

Driver	Average velocity error (m/s)	
	LC	CA
1	0.6892	0.5901
2	0.3870	0.4675
3	0.9424	0.4123
4	0.9424	0.2809
5	0.6580	1.6195
6	0.5227	3.1795
7	0.7033	0.6573
8	0.8877	0.3308
9	0.3535	0.1506
10	0.6439	0.2194
11	0.8413	0.7884
12	0.6881	0.2135
13	0.4204	2.5184
14	0.0645	0.2558
15	0.3761	0.0418
16	0.2395	0.0849
17	0.5581	0.2351
18	0.2430	0.4315
19	0.4498	0.1559
20	0.7365	1.0612
AVG	**0.5674**	**0.6847**

desired path. Note: this curvature is based on the absolute longitudinal distance, X, not relative distance Δx. As one can see from Fig. 13, the free-flow motor primitive is active leading up to the curve. Once the optimal control input for the curve motor primitive, $j_c(t)$, reaches a value that is less than the free-flow motor primitive optimal control, $j_f(t)$, the curve motor primitive becomes active and starts to decelerate for the upcoming curvature in the driver's desired path. Once the maximum curvature is reached, the free-flow motor primitive is then activated to ramp the driver up to the desired speed. The second minimum velocity from the Two-thirds law is always chosen because this corresponds to the curvature that the driver is going to be able to react to and achieve after the sudden collision-avoidance maneuver. The first minimum velocity based on the curvature is desired by the driver; however, it is unobtainable due to the limits on deceleration due to braking. The average velocity error for all twenty drivers can be seen in Table 3.

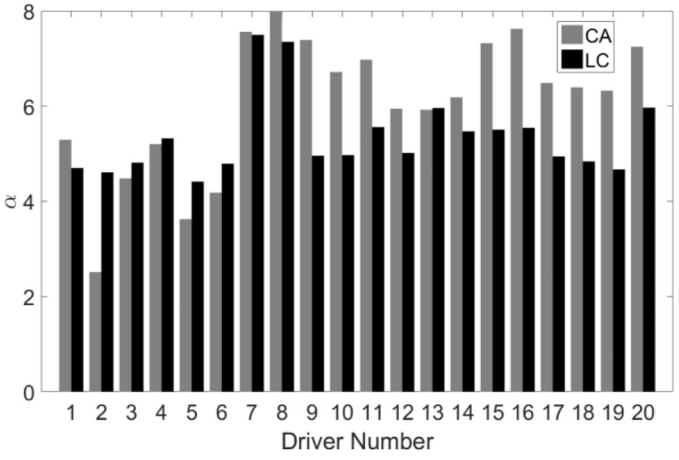

Fig. 14. Feedforward longitudinal driver model parameter α.

The results show that the feedforward longitudinal driver model is capable of reproducing most of the driver's velocities during the LC and CA maneuvers. For a few drivers, such as Driver 5, 6, and 13, there is a high average velocity error. This is due to the fact that some drivers rely on car-following feedback to control their velocities. This results in the need for an integrated feedforward and feedback longitudinal driver model. Model parameters for the twenty subjects are shown in Figs. 14 and 15 where once again the dissimilarities among different drivers are obvious.

4.3. Integrated lateral and longitudinal driver model results

The performances of the integrated lateral and longitudinal driver model are presented in this section. Fig. 16 shows the integrated longitudinal driver model fit for a CA maneuver for two drivers and Fig. 17 shows the driver's position weighted transition gain. The

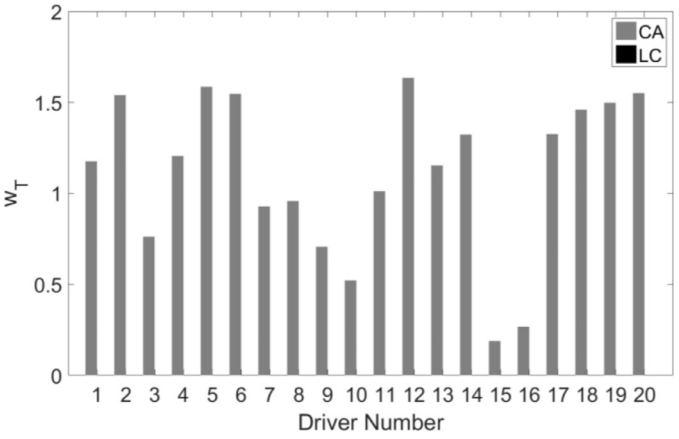

Fig. 15. Feedforward longitudinal driver model parameter w_T.

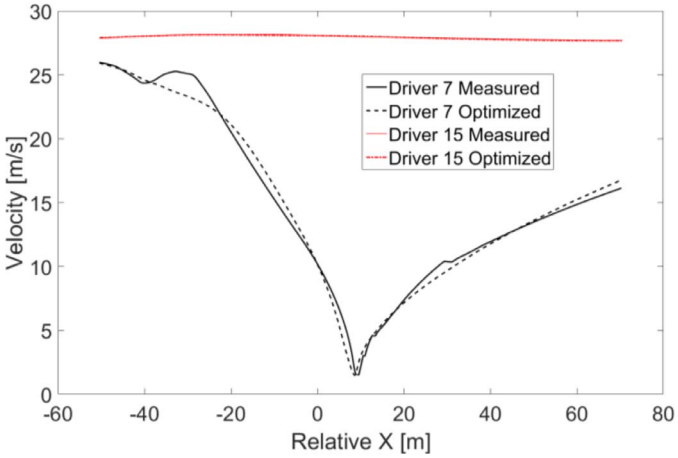

Fig. 16. Driver's combined feedforward and feedback longitudinal model for a CA maneuver.

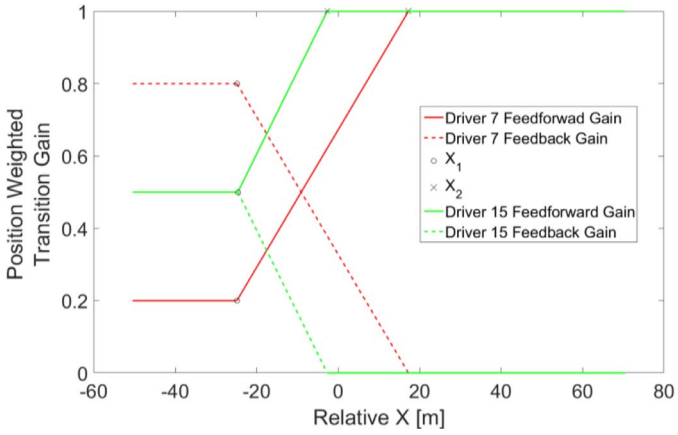

Fig. 17. Driver's combined longitudinal model position weighted transition gain for the CA maneuver in Fig. 16.

Table 4
Integrated lateral and longitudinal driver model performances.

Driver	Steering wheel angle goodness of fit		Average velocity error (m/s)	
	LC	CA	LC	CA
1	0.88	0.93	0.423	0.318
2	0.79	0.81	0.524	0.529
3	0.74	0.81	0.813	0.533
4	0.77	0.84	0.651	0.321
5	0.88	0.94	0.424	0.480
6	0.90	0.93	0.285	0.403
7	0.77	0.80	0.910	0.492
8	0.71	0.79	0.848	0.383
9	0.94	0.91	0.311	0.106
10	0.87	0.85	0.191	0.122
11	0.71	0.77	0.404	0.227
12	0.93	0.93	0.285	0.283
13	0.87	0.90	0.546	0.379
14	0.94	0.95	0.267	0.229
15	0.93	0.92	0.205	0.082
16	0.92	0.92	0.275	0.106
17	0.92	0.93	0.287	0.205
18	0.92	0.94	0.320	0.265
19	0.93	0.93	0.298	0.220
20	0.95	0.94	0.215	0.224
AVG	**0.86**	**0.89**	**0.424**	**0.295**

average velocity errors and steering wheel angle goodness of fit for all twenty drivers in LC and CA maneuvers can be seen in Table 4. The integrated longitudinal driver model was able to replicate all twenty

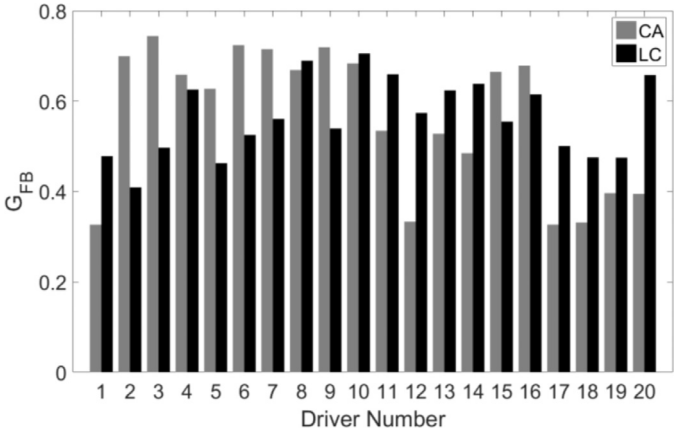

Fig. 18. Feedback longitudinal driver model parameter G_{FB}.

driver's velocity for LC and CA maneuvers with an average error of less than 0.45 m/s (1 mph). Using the integrated longitudinal driver model, the velocity errors for Driver 5, 6, and 13 were greatly reduced over using only the feedforward driver model. Fig. 18 shows the parameters optimized with individual drivers' data.

5. Conclusions

This paper focuses on the modeling of steering wheel angle and vehicle velocity choice for individual drivers for a variety of driving maneuvers. The goal of these models is to accurately represent a driver's control actions in real-world driving scenarios, with a focus on collision-avoidance maneuvers, so that ADAS may incorporate this information to provide driver-specific control intervention and warnings. Human driver data are collected in a driver simulator, and simulation studies are used to validate the proposed driver models. An integrated feedback and feedforward longitudinal driver model was presented that works with the existing lateral driver model and the driver's desired path. The feedback model is a linear car-following model that is adapted to work with the combined lateral driver model and desired path by using the relative following distance and speed. As a standalone driver model, the feedforward longitudinal driver model is capable of replicating most drivers' velocities during LC and CA maneuvers. However, the model has large average velocity errors for a few drivers resulting in the need for a combined feedforward and feedback longitudinal driver model. The feedforward longitudinal driver model takes into account the driver's velocity regulation based on the curvature along their desired path. This combined feedback and feedforward longitudinal driver model is representative of a human driver's velocity control task. This new combined longitudinal driver model is able to accurately model all twenty drivers' velocities during LC and CA maneuvers with less than 0.45 m/s (1 mph) average error. From the clear dissimilarity among driver model parameters, the need for a driver and maneuver specific longitudinal driver model parameters is obvious. This means a one-size-fits-all driver model is inadequate because different drivers have different driving styles. Also, driving style is maneuver dependent i.e., the same driver acts differently for a standard lane change than they would in a collision-avoidance maneuver.

Acknowledgment

This research is partially supported by National Science Foundation Cyber-Physical Systems (NSF-CPS) Award 1645657.

References

[1] Continental automotive -emergency steer assist, Continental-automotive.com, 2016.

[Online]. Available: http://www.continental-automotive.com/www/automotive_de_en/themes/passenger_cars/chassis_safety/ausweichassistent_en.html [Accessed: 24- Mar- 2016].
[2] Schnelle S, Wang J, Su H, Jagacinski R. A driver steering model with personalized desired path generation. IEEE Trans Syst Man Cybern 2017;47(1):111–20.
[3] Schnelle S, Wang J, Su H, Jagacinski R. A personalizable driver steering model capable of predicting driver behaviors in vehicle collision avoidance maneuvers. IEEE Trans Hum-Mach Syst 2017;47(5):625–35.
[4] MacAdam CC. Understanding and modeling the human driver. Veh Syst Dyn: Int J Veh Mech Mobil 2003;40:101–34.
[5] McRuer DT, Allen RW, Weir DH, Klein RH. New results in driver steering control models. Hum Factor 1977;19(4):381–97.
[6] Weir DH, McRuer DT. Dynamics of driver vehicle steering control. Automatica 1970;6:87–98.
[7] McRuer DT. Human dynamics in man-machine systems. Automatica 1980;16:237–53.
[8] MacAdam CC. An optimal preview control for linear systems. J Dyn Syst Meas Control ASME 1980;102:188–90.
[9] Odhams AMC, Cole DJ. Application of linear preview control to modelling human steering control. J Automob Eng 2009;223:835–53.
[10] Cole DJ, Pick AJ, Odhams AMC. Predictive and linear quadratic methods for potential applications to modelling driver steering control. Veh Syst Dyn 2006;44:259–84.
[11] Ungoren AY, Peng H. An adaptive lateral preview model. Veh Syst Dyn 2006;43:245–59.
[12] Keen SD, Cole DJ. Bias-free identification of a linear model-prediction steering controller from measured driver steering behavior. IEEE Trans Syst Man Cybern 2012;42:434–43.
[13] T. Qu, H. Chen, Y. Ji and H. Guo, “Modeling driver steering control based on stochastic model predictive control,” in IEEE Int. conf. on systems, man, and cybernetics, Manchester, England, October 13-16, 013, pp. 3704–3709.
[14] Zafeiropoulos S. Design on a lane-tracking driver steering assist system and its interaction with a two-point visual driver model. American control conference, Portland, OR, June 4-6. 2014. p. 3911–7.
[15] Prokop G. Modeling human vehicle driving by model predictive online optimization. Veh Syst Dyn 2001;35(1):19–53.
[16] Flad M, Trautmann C, Diehm G, Hohmann S. Experimental validation of a driver steering model based on switching of driver specific primitives. IEEE international conference on systems, man, and cybernetics, Manchester, England, October 13-16. 2013. p. 214–20.
[17] Huang J, Tan H, Bu F. Preliminary steps in understanding a target and control based driver steering model. American control conference, San Francisco, CA, June 29-July 1. 2011. p. 5243–8.
[18] Mihaly A, Gaspar P. Identification of a linear driver model based on simulator experiments. *International symposium on applied computational intelligence and informatics*, Timisoara, Romania, May 15-17. 2014. p. 13–8.
[19] Tokutake H, Sugimoto Y, Shirakata T. Real time identification method of driver model with steering manipulation. Veh Syst Dyn 2012;51:109–21.
[20] Chai YW, Abe Y, Kano Y, Abe M. A study on adaptation of SBW parameters to individual driver's steer characteristics for improved driver-vehicle system performance. Vehicle Syst Dyn 2007;44:874–82.
[21] Plöchl M, Edelmann J. Driver models in automobile dynamics application. Veh Syst Dyn 2007;45:699–741.
[22] Brackstone M, McDonald M. Car-following: a historical review. Transp Res Part F 1999;2(4):181–96.
[23] Panwai S, Dia H. Comparative evaluation of microscopic car-following behavior. Intell Transp Syst, IEEE Trans 2005;6(3):314–25.
[24] Lee K, Peng H. Identification and verification of a longitudinal human driving model for collision warning and avoidance systems. Int J Veh Autonom Syst 2004;2(1):3–17.
[25] Chandler RE, Herman R, Montroll EW. Traffic dynamics: studies in car following. Oper Res 1958;6(2):165–84.
[26] Pipes LA. An operational analysis of traffic dynamics. J Appl Phys 2004;24(3):274–81.
[27] Gazis DC, Herman R, Rothery RW. Nonlinear follow-the-leader models of traffic flow. Oper Res 1961;9(4):545–67.
[28] Kometani, E., and Sasaki, T., “Dynamic behaviour of traffic with a non-linear spacing-speed relationship,” pp. 105–109, 1959.
[29] Helly, W., “Simulation of bottlenecks in single-lane traffic flow,” pp. 207–238, 1959.
[30] Tyler JS. The characteristics of model following systems as synthesizes by optimal control. IEEE Trans Autom Control 1964;AC-9:485–98.
[31] Saifuzzaman Mohammad, Zheng Zuduo. Incorporating human-factors in car-following models: a review of recent developments and research needs. Transp Res Part C 2014;48:379–403.
[32] Kim JH, Hayakawa S, Suzuki T, Hayashi K, Okuma S, Tsuchida N, Kido S. Modeling of driver's collision avoidance maneuver based on controller switching model. Syst Man Cybern Part B IEEE Trans 2005;35(6):1131–43.
[33] Sekizawa S, Inagaki S, Suzuki T, Hayakawa S, Tsuchida N, Tsuda T, Fujinami H. Modeling and recognition of driving behavior based on stochastic switched ARX model. Intell Transp Syst IEEE Trans 2007;8(4):593–606.
[34] Kishimoto Y, Oguri K. A modeling method for predicting driving behavior concerning with driver's past movements. Vehicular electronics and safety, 2008. ICVES 2008. IEEE international conference on. 2008. p. 132–6.
[35] Okamoto M, Otani S, Kaitani Y, Uchida K. Identification of driver operations with extraction of driving primitives. Control applications (CCA), 2011 IEEE international conference on. 2011. p. 338–44.
[36] Okuda H, Ikami N, Suzuki T, Tazaki Y, Takeda K. Modeling and analysis of driving behavior based on a probability-weighted arx model. Intell Transp Syst IEEE Trans 2013;14(1):98–112.
[37] Zhao G, Wu C. Mathematical modeling of driver speed control with individual differences. IEEE Trans Syst Man Cybern 2013;43(September (5)):1091–104.
[38] Bifulco GN, et al. Driving behaviour models enabling the simulation of advanced driving assistance systems: revisiting the action point paradigm. Transp Res Part C 2013;36:352–66.
[39] Pariota L, Bifulco GN. Experimental evidence supporting simpler Action Point paradigms for car-following. Transp Res Part F 2015;35:1–15.
[40] Pariota L, Bifulco GN, Brackstone M. A linear dynamic model for driving behavior in car following. Transp Sci 2015;50(3):1032–42.
[41] Spena MR, Timpone F, Farroni F. Virtual testing of advanced driving assistance systems. Int J Mech 2015;9:300–8.
[42] Eggert J, Damerow F, Klingelschmitt S. The foresighted driver model. 2015 *IEEE intelligent vehicles symposium (IV)*. 2015. p. 322–9.
[43] Wang J, Zhang L, Zhang D, Li K. An adaptive longitudinal driving assistance system based on driver characteristics. IEEE Trans Intell Transp Syst 2013;14(March (1)):1–12.
[44] Butakov VA, Ioannou P. Personalized driver/vehicle lane change models for ADAS. 64. 2015. p. 4422–31.
[45] Jain A, Koppula HA, Raghavan B, Soh S, Saxena A. Car that knows before you do: anticipating maneuvers via learning temporal driving models. IEEE international conference on computer vision (ICCV). 2015. p. 3182–90.
[46] Jurecki R, Stariczyk TL. Driver Model for the analysis of pre-accident situations. Veh Syst Dyn 2009;47:589–612.
[47] Choi J, Yi K. Design and evaluation of emergency driving support using motor driven power steering and differential braking on a virtual test track. *SAE Int J Passenger Cars - Mech Syst* 2013;6(2):691–704.
[48] Hong, T., Kwon, J., Park, K., Lee, K. et al., "Development of a driver's intention determining algorithm for a steering system based collision avoidance system," *SAE Technical Paper* 2013-01-0054, 2013.
[49] Wu M, Deng W, Zhang S, Sun H. Modeling and simulation of intelligent driving with trajectory planning and tracking. SAE Int J Trans Saf 2014;2(1):1–7.
[50] Falcone P, Ali M. Predictive threat assessment via reachability analysis and set invariance theory. IEEE Trans Intell Tranp Syst 2011;12:1352–61.
[51] Sentouh C, Chevrel P, Mars F, Claveau F. A sensorimotor driver model for steering control. IEEE int. conference on systems, man, and cybernetics, San Antonio, TX, October. 2009. p. 2462–7.
[52] Saleh L, Chevrel P, Claveau F, Lafay J-F, Mars F. Shared steering control between a driver and an automation: stability in the presence of driver behavior uncertainty. IEEE Trans Intell Transp Syst 2013;14:974–83.
[53] Khodayari A, Ghaffari A, Kazemi R, Braunstingl R. A modified car-following model based on a neural network model of the human driver effects. IEEE Trans Syst Man Cybern Part A 2012;42(November (6)):1440–9.
[54] Shi B, Xu L, Hu J, Tang Y, Jiang H, Meng W, Liu H. Evaluating driving styles by normalizing driving behavior based on personalized driver modeling. IEEE Trans Syst Man Cybern 2015;45(December(12)):1502–8.
[55] Guozhen Z, Changxu W. Mathematical modeling of driver speed control with individual differences. IEEE Trans Syst, Man Cybern 2013;43(September (5)):1091–104.
[56] Prynne K, Martin P. Braking behavior in emergencies SAE International; 1995. *SAE Technical Paper*, no. 950969.
[57] Lechner D, Malaterre G. Emergency maneuver experimentation using a driving simulator. SAE International; 1991. *SAE Technical Paper*, no. 910016.
[58] Choi J, Yi K. Design and evaluation of emergency driving support using motor driven power steering and differential braking on a virtual test track. SAE Int J Passeng Cars – Mech Syst 2013;6:694–704. no. 2013-01-0726.
[59] Xu G, Liu L, Song Z, Ou Y. Generating lane-change trajectories using the dynamic model of driving behavior. IEEE int. conference on information and automation, Shenzhen, China, June. 2011. p. 464–9.
[60] Yao W, Zhao H, Davoine F, Zha H. Learning lane change trajectories from on-road driving data. IEEE intelligent vehicles symposium, Alcala de Henares, Spain, June 3-7. 2012. p. 885–90.
[61] Rucco A, Notarstefano G, Hauser J. Computing minimum lap-time trajectories for a single-track car with load transfer. Proceedings of the IEEE conference on decision control, Maui, HI, USA, December. 2012. p. 6321–6.
[62] Timings JP, Cole DJ. Efficient minimum manoeuvre time optimisation of an oversteering vehicle at constant forward speed. Proceedings of the American control conference. 2011.
[63] Velenis E, Tsiotras P. Minimum-time travel for a vehicle with acceleration limits: theoretical analysis and receding-horizon implementation. J Optim Theory Appl 2008;138(2):275–96.
[64] Berntorp K. Derivation of a six degrees-of-freedom ground-vehicle model for automotive applications. Department of Automatic Control, Lund University; February 2013.
[65] Pacejka HB, Bakker E. The magic formula tyre model. Veh Syst Dyn 1992;21:1–18.
[66] Levison WH, et al. Development of a driver vehicle module for the interactive highway safety design model. Washington, DC, USA: Federal Highway Admin.;

2007 Tech. Rep. USDOT-FHWA-HRT-08-019, Nov. [Online]. Available: http://www.fhwa.dot.gov/publications/research/safety/08019/08019.pdf.
[67] Winsum WV, Godthelp H. Speed choice and steering behaviour in curve driving. Hum Factors 1996;38(September (3)):434–41.
[68] Reymond G, Kemeny A, Droulez J, Berthoz A. Role of lateral acceleration in curve driving: driver model and experiments on a real vehicle and a driving simulator. Hum Factors J Hum Factors Ergon Soc 2001;43(June (3)):483–95.
[69] Flash T, Meirovitch Y, Barliya A. Models of human movement: trajectory planning and inverse kinematics studies. Robot Autonom Syst 2013;61(April (4)):330–9.
[70] Bosetti P, Da Lio M, Saroldi A. On curve negotiation: from driver support to automation. IEEE Trans Intell Transp Syst 2015;16(August (4)):2082–93.